# Supporting Information for:

# Detection of Protein−Small Molecule Binding Using a Self-Referencing External Cavity Laser Biosensor

Meng Zhang,[†] Jessie Peh,[‡] Paul J. Hergenrother,[‡] and Brian T. Cunningham[§,⊥]

[†]Department of Physics, [‡]Department of Chemistry, [§]Department of Bioengineering, and [⊥]Department of Electrical and Computer Engineering, University of Illinois at Urbana−Champaign, Urbana, Illinois 61801, United States

## Supporting Information Table of Contents



## Section 1. Thermal Noise and Nonspecific Binding

Noise sources including thermal fluctuations and nonspecific binding can lead to lasing wavelength value (LWV) shifts which are indistinguishable from the signals generated by an actual binding event. Among these noise sources, thermal noise is the main limiting factor on the external cavity laser (ECL) biosensor's resolution performance when the reference sensor is not used in conjunction with the active sensor.

Temperature fluctuations have two main effects on the sensor system: (1) shift the gain profile of the semiconductor optical amplifier (SOA), and (2) modulate the dimensions and the refractive index of the photonic crystal (PC) materials. The gain profile of the SOA is extremely sensitive to temperature changes. We observed LWV shifts with a fluctuation range of 15 pm even with a commercial SOA temperature control unit with temperature stability of 0.1°C. This large thermal noise makes it necessary to have a reference sensor that shares the same SOA to experience the same wavelength shifts caused by SOA temperature fluctuations. The PC materials used in this work and the test samples are also sensitive to ambient temperature fluctuations due to thermal expansion/contraction (characterized by coefficient of

thermal expansion) and thermal-opto effects (characterized by thermal-optic coefficient). We have used rigorous coupled-wave analysis computer simulations to study the effect of a small sensor temperature change on the peak wavelength of the PC. For example, a temperature change of 0.05°C results in a LWV shift of 0.1 pm due to the thermal-opto effect[1] of the $TiO_2$ coating, and could result in a LWV shift of 9.0 pm due to the thermal expansion of UVCP. It's critical to compensate the thermal noise experienced by the PC via an identical reference sensor that is in close proximity to the active sensor and shares the same thermal environment.

In the reference well, no protein is functionalized on the surface. Thus the LWV recorded for that well reflects both thermal noise and nonspecific binding of small molecules on the GA-functionalized surface. By subtracting the LWV of the reference well from that of the active well, part of the nonspecific binding to GA surface can be compensated. Also, from Table 1, noninteracting protein-small molecule interaction results in LWV shifts in the range of -2.4–2.6 pm which are all within 3σ (Figure S2) of the noise generated when only buffer solution was added to the sensor and reference wells.

**Section 2. Path to High Throughput**

As an initial demonstration of the technology's capabilities, in the screen with CA II, we performed the tests in serial with the throughput of 3 tests per hour. However, throughput was increased through demonstration of screening 6 compounds at a time within a single well (Figure 3), effectively resulting in a screening throughput of 18 compounds/hour.

It is our intention, with this initial demonstration of the technology, to demonstrate the capability for high throughput, which can be achieved by simple engineering of the instrument and test method. For example, our approach is based on the fact that, in an initial screening to identify small molecule binders to target proteins, we need the LWVs at the initial time point and at the end point to obtain the LWV shifts, rather than LWVs in the whole binding process. Thus, we are able to take initial LWV readings from each well in a microplate to determine the pre-binding wavelength before introduction of small molecules.

After introduction of small molecules, a second scan of the microplate can be used to gather final LWVs for the wells. As each LWV measurement only takes <0.1 seconds, the rate of measurement is limited by the rate of the motion stage that moves the microplate over the optical detection head. Using our current system with a single optical fiber detection head, we estimate that an entire 384-well plate can be scanned in ~3 minutes. Including time for stabilization of the binding interaction, a 384-well plate, screening with 10 compounds/well, with one reference sensor for each active sensor, could screen 1,920 compounds in 15 minutes.

Besides utilizing the end-point reading method, the throughput may be further increased by using multiple SOA in parallel to perform multiple tests at the same time. Although the cost of each SOA is ~$5000, the costs of implementation of an 8-channel detection instrument is consistent with the costs of current HTS instruments.

## Section 3. Materials and Methods

### Materials

All chemicals and reagents were purchased from Sigma-Aldrich (St. Louis, MO) unless otherwise noted. Biosensor plates were a gift from SRU Biosystems (Woburn, MA).

### Sensors and Detection Instrument

The sensor surface is a one-dimensional photonic crystal (PC). The fabrication process of PC biosensors using nanoreplica molding has been described in previous published work[2] and is briefly introduced below. An 8-inch silicon wafer with grating structure etched permanently into its surface is used as the master wafer, and the structure is replicated onto a thin layer of UV curable epoxy on a polyester sheet, followed by depositing a thin layer of $TiO_2$ high refractive index material. The flexible substrate with the imprinted PC structure is attached with adhesive onto the bottom surface of standard 96-, or 384-well microtiter plates. In this work, we design the PC with period $\Lambda$ = 550 nm, grating depth $h$ = 170 nm, and with $TiO_2$ thickness $t_{TiO2}$= 100 nm. The PC structure, when covered with water, shows a

resonant peak at near infrared (NIR) region with peak reflection wavelength $\lambda$ = 856 nm and full-width at half maxim of $\Delta\lambda$ = 3 nm.

The external cavity laser (ECL) cavity is formed by the PC resonant reflector and a NIR broadband mirror, where the PC serves as the wavelength selective element.[3] Optical gain is provided by a fiber coupled semiconductor optical amplifier SOA (SAL-372-850, Superlum Inc., $\lambda_0$ = 850 nm and a 3 dB bandwidth of $\Delta\lambda$ = 40 nm). Light comes from one end of the fiber is reflected against the NIR mirror, while light from the other end of the fiber, after a collimating lens, is directed to a polarizing cube beamsplitter. The incident polarization is adjusted so that the outcoming s- and p-polarized light from the cube have equal intensity. A half-wave plate is then used to switch the s-polarized light to p-polarized light. Both beams, with equal intensity, illuminate two adjacent sensor wells at normal incidence through the bottom of the microplate, respectively, with polarization direction perpendicular to the grating direction. The illuminated regions have an approximately 400-$\mu$m-diameter. The narrow linewidth reflection of the two PCs is coupled back to the laser cavity and gets amplified by the SOA. An active optical resonator with two resonant modes is established and achieves dual-mode operation with narrow lasing linewidth through stimulated emission process. A small portion of light is directed out from the cavity to a detection system to monitor the LWV in real time. Figure S1 shows the dual-mode lasing spectrum of the ECL system, with one well immersed in DI water, and the other well immersed in 10% DMSO solution.

**Overexpression and purification of GST-XIAP**

The cDNA encoding human X-linked inhibitor of apoptotic protein (XIAP) was provided by Dr. Colin Duckett (University of Michigan) in a pGEX vector. The pGEX-XIAP vector was transformed into electrocompetent BL21(DE3) *E. coli* and protein expression was induced at $OD_{600}$ of 0.4 via the addition of IPTG to 0.1 mM at 18 ℃ for 18 h. Bacteria were harvested by centrifugation and stored at -20 ℃. Pellets stored at -20 ℃ were thawed at 25 ℃ in 13 mL of binding buffer (1X PBS + 1 mM DTT) with 1 mM phenylmethanesulfonyl fluoride (PMSF) and 1X protease inhibitor cocktail (Cell Signaling

Technology). Bacteria were lysed by sonication, centrifuged at 35,000 x *g* for 30 min at 4 °C, and incubated with 1 mL glutathione Sepharose 4B (GE Biosciences) slurry for 1 h at 4 °C. Resin was washed with an additional 40 mL of binding buffer, followed by elution with 10 mL of elution buffer (50 mM Tris pH 8.0 + 10 mM glutathione). GST-XIAP was buffer exchanged into XIAP assay buffer (10 mM HEPES, 150 mM NaCl, 20 $\mu$M EDTA, 0.005% Tween 20, pH 7.4) and concentrated using Amicon 50K MWCO (EMD Millipore) spin concentrator. Protein concentration was determined by Bradford assay and stored in XIAP assay buffer at 4 °C for short term storage.

**Surface chemistry**

PC biosensor surface was functionalized first with a polyvinylamine layer (PVA; provided by SRU Biosystems Inc.) using a 10% PVA solution in 1X PBS and incubated at 37 °C for 4 h. The wells were then washed thrice with 1X PBS before an additional functionalization with glutaraldehyde (GA). The wells were incubated with a 25% GA solution in 1X PBS for 4 h at 37 °C. After 4 h, the wells were washed thrice with 1X PBS.

To immobilize the protein of interest onto the biosensor surface, 40 µL of 1 mg/mL of protein solution was added to each of the active well and incubated overnight at 4 °C. Streptavidin (SA, ProZyme), bovine carbonic anhydrase isozyme II (CA II) and human serum albumin (HSA) were diluted in 1X PBS pH 7.4. Lyophilized recombinant human NAD(P)H dehydrogenase quinone 1 (NQO1) was dissolved with 100 mM potassium phosphate buffer at pH 7.4. Purified human lactate dehydrogenase isoform 5 (hLDH5, hLDH-A, mybiosource.com) was diluted in 100 mM sodium phosphate buffer at pH 7.4. GST-XIAP was diluted in XIAP assay buffer. Caspase-3 was diluted in caspase activity buffer (50 mM HEPES, 300 mM NaCl, pH 7.4). After an overnight incubation, the wells were washed once to remove excess unbound protein and kept in their respective buffers at 4 °C till they were used. A blocking step was not incorporated in the small molecule detection assay. Since the nonspecific binding observed was very low even without a blocking step, this step was eliminated for the sake of simplifying the assay protocol.

**Biotin and SA binding assay**

Biotin dissolved in 1X PBS was added to both the control and sensing wells at a final concentration of 75 $\mu$g/mL. Biotin was allowed to incubate with SA and the sensor plate was read for 20 min at RT.

**Protein−small molecule binding assays**

The cognate small molecules of interest: dorzolamide, warfarin, SM-122, SM-164 (gift from Prof. Shaomeng Wang, U. Michigan), NHI-1, 1b and 1g (gift from Prof. Filippo Minutolo, U. Pisa) and Q-VD-O-Ph (EMD Millipore) were dissolved in DMSO. Dicoumarol (gift from Prof. David Boothman, UTSW) was dissolved in basic water. The small molecules were added at a final concentration of 50 $\mu$M in 5% DMSO (1% DMSO for warfarin) into both the active and reference wells for all of the binding assays. The sensor plate was read for 5-20 min at RT.

**Dose response binding assays**

Dorzolamide dissolved in 5% DMSO in 1X PBS was added to both the active and reference wells at five final concentrations of ranging from 200 $\mu$M to 2 nM. The sensor plate with CAII immobilized on the active wells was read for 20 min at RT. Warfarin dissolved in 1% DMSO in 1X PBS was added to both the control and sensing wells at five final concentrations of ranging from 200 $\mu$M to 2 nM. The sensor plate with HSA immobilized on the active wells was read for 5-10 min at RT.

**High-throughput screen**

A collection of 48 compounds from an in-house library in 10 mM DMSO was used for the screen, with dorzolamide a known inhibitor of CAII spiked in. The compounds were added to both the active and reference wells and screened at a final concentration of 50 $\mu$M in 5% DMSO in 1X PBS. Acetazolamide at a final concentration of 50 $\mu$M in 5% DMSO in 1X PBS was used as the positive control. 5% DMSO in 1X PBS was used as the negative control. The sensor plate with CAII immobilized on the active wells was read for 20 min at RT to obtain the binding data.

**Specific binding assay for HSA and warfarin**

A 1% DMSO solution in 1X PBS containing 5 structurally unrelated small molecules in addition to warfarin was added to both sensing well with immobilized HSA and control well at a final concentration

of 25 $\mu$M. To eliminate the possibility of nonspecific binding, the 5 other small molecules were added separately to both the sensing and control wells. The sensor plate was read for 5-10 min at RT.

**Data analysis:**

The Z' factor was calculated to determine the quality of the screening assay, with σ the standard deviation, and μ the mean, of positive and negative controls.[4]

$$Z' = 1 - \frac{3(\sigma_p + \sigma_n)}{|\mu_p + \mu_n|}$$

**Section 4. Supporting Figures S1-S7 and Table S1**

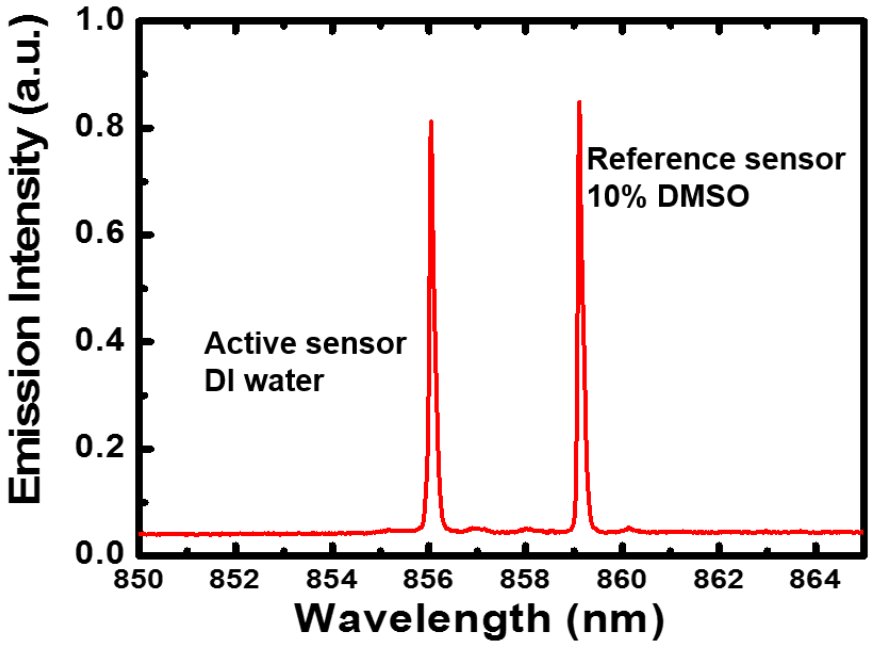


**Figure S1.** Dual-mode lasing spectrum of the self-referencing external cavity laser.

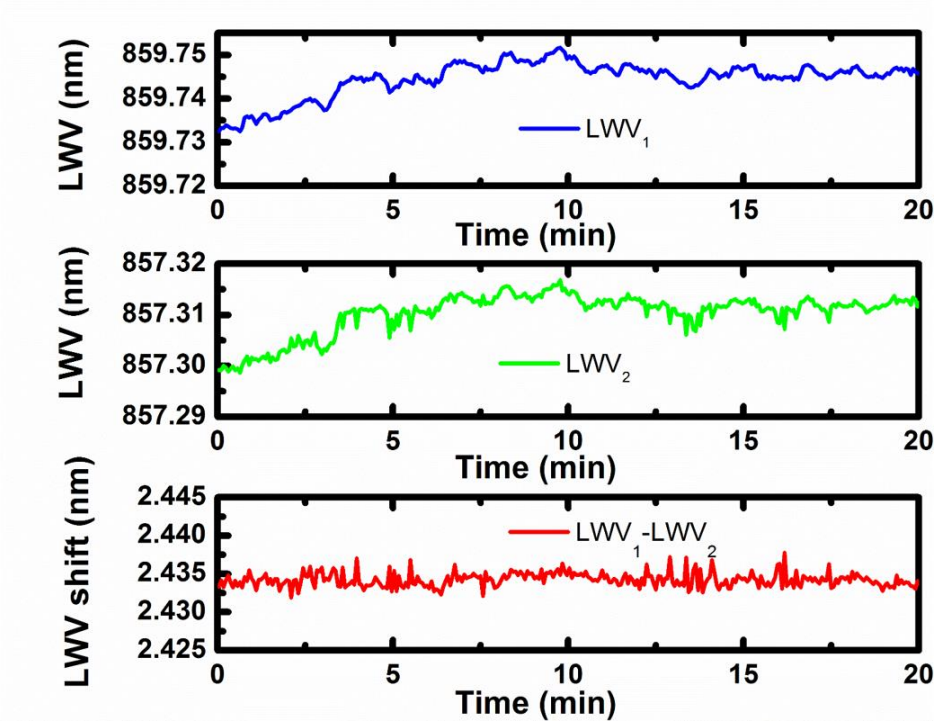


**Figure S2.** Compensation of environmental fluctuations via the subtraction of LWV of the reference well (green) from the LWV of the active well (blue). The resulting LWV shift (red) has a reduced noise level with standard deviation of 0.8 pm in a 20 minute measurement.

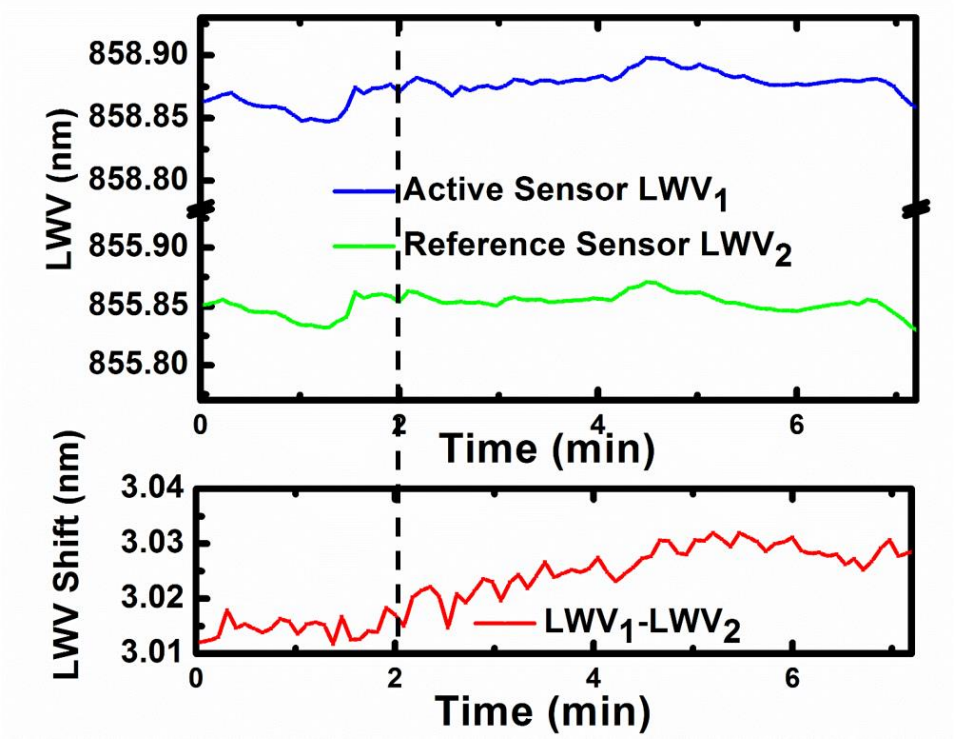


**Figure S3.** Binding of biotin (75 $\mu$g/mL) to immobilized SA. LWV shift due to the binding of biotin to SA (red) was obtained by subtracting the LWV of the reference well (green) from that of the active well with immobilized SA (blue). Dotted line indicates the addition of biotin to both the active and reference wells.

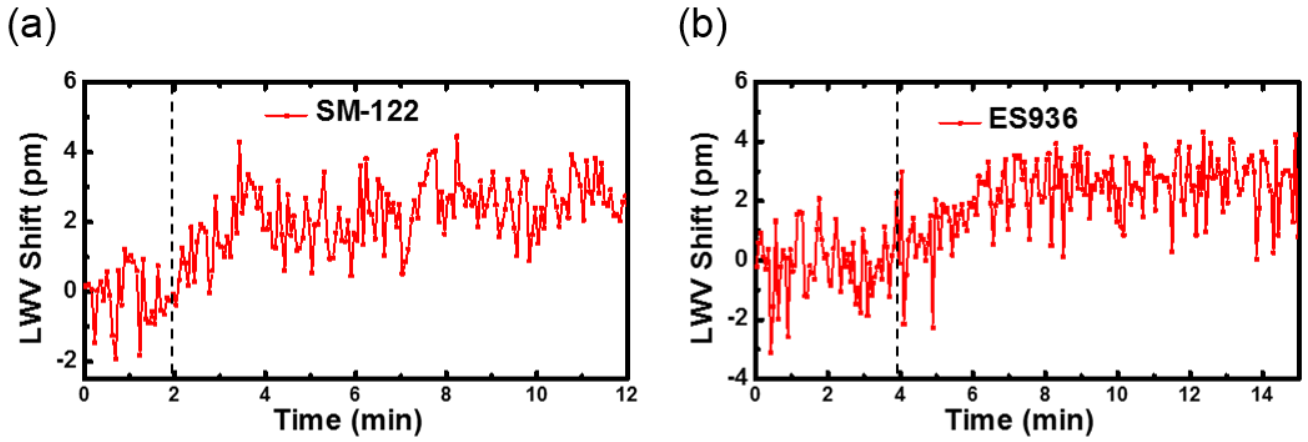


**Figure S4.** LWV shift due to the binding of 50 $\mu$M small molecules to immobilized target proteins. (a) SM-122 and GST-XIAP, (b) ES936 and NQO1. Dotted line indicates the addition of small molecules to both the active and reference wells.

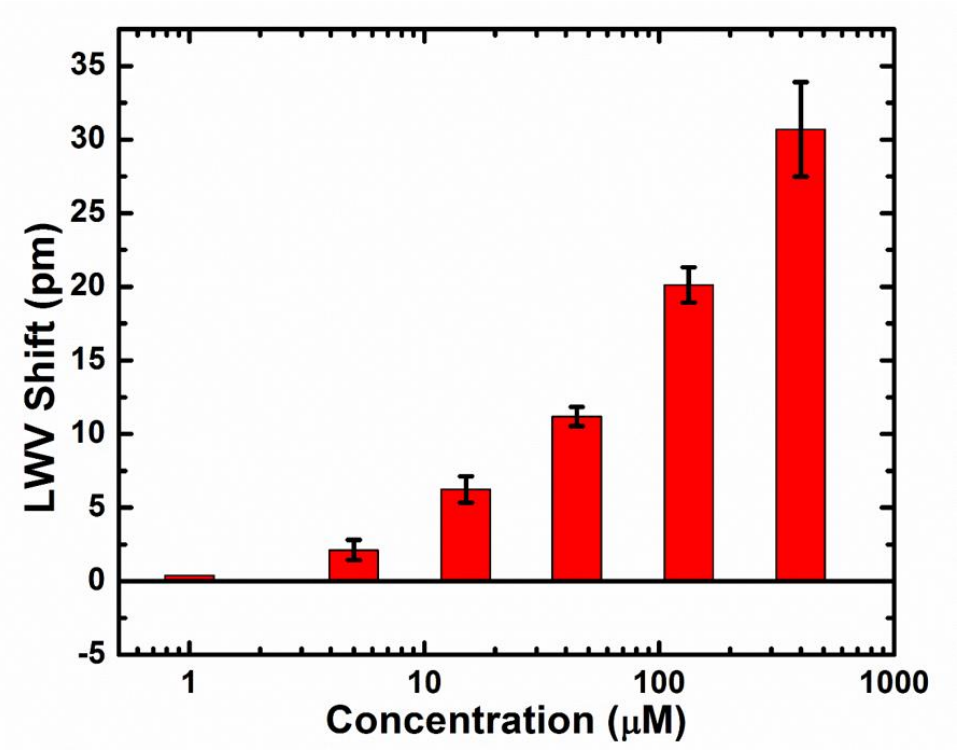


**Figure S5.** Dose response binding of warfarin to immobilized HSA. Error bars represent the standard error of mean of at least three independent experiments.

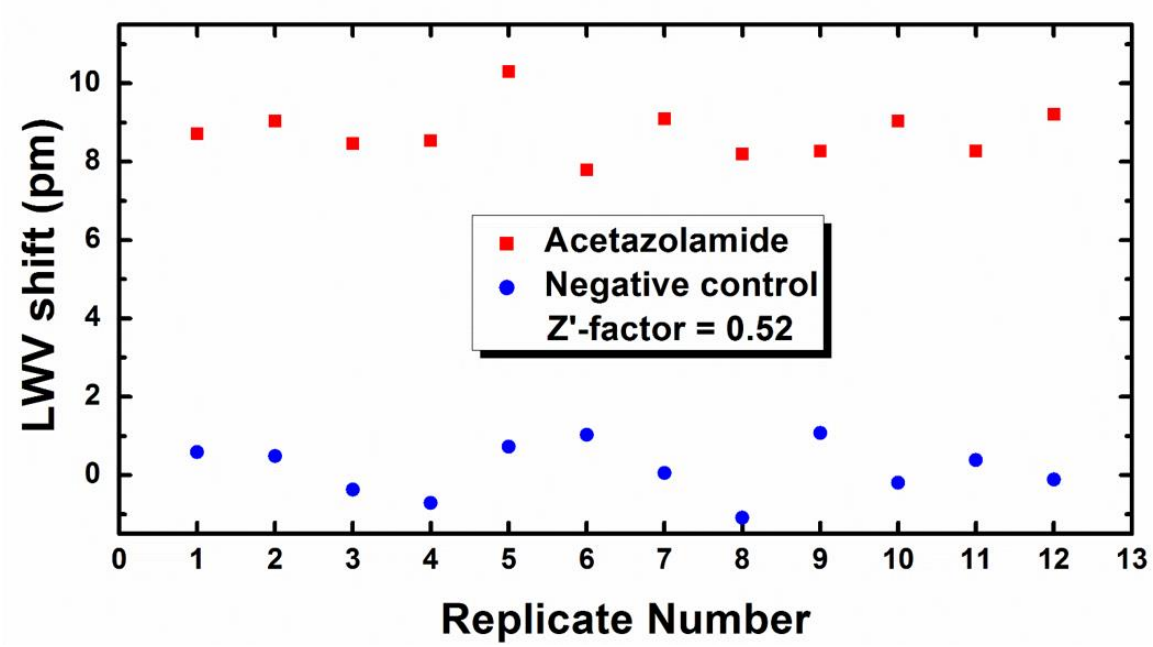


**Figure S6.** Determination of Z'-factor for the self-referencing ECL biosensor assay with immobilized CA II. 50 $\mu$M acetazolamide (5% DMSO) was used as the positive control; 5% DMSO in PBS was used as the negative control.

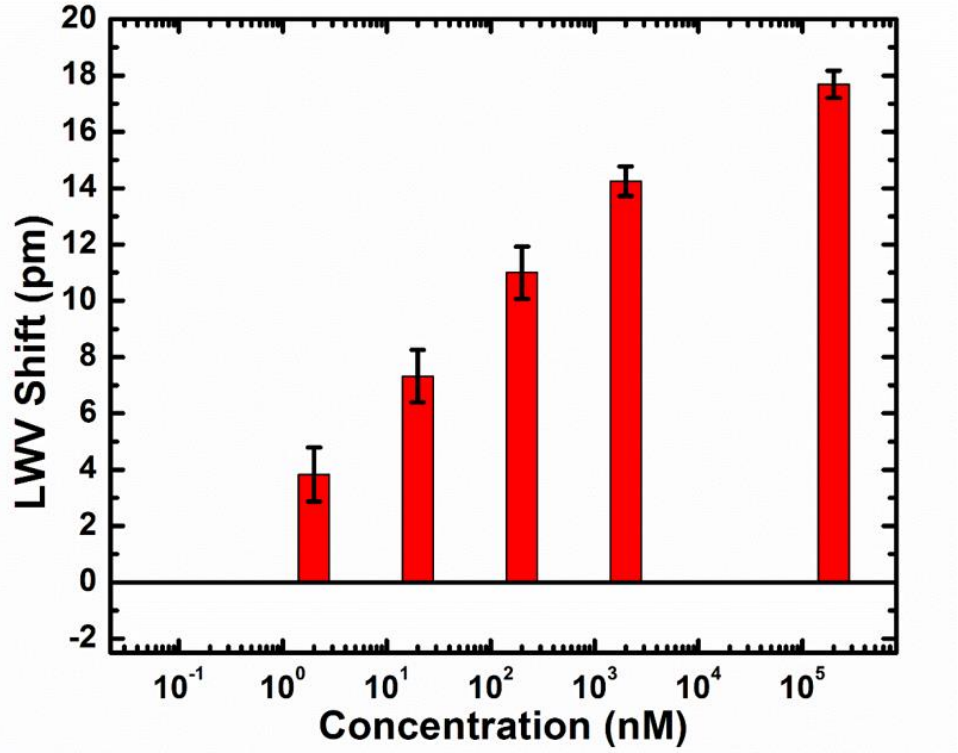


**Figure S7.** Dose response binding of dorzolamide to immobilized CA II. Error bars represent the standard error of mean of at least three independent experiments.

**Table S1. Figure of merit table**

| Methods | *Q*-factor | Sensitivity (nm· $RIU^{-1}$) | FOM = *Q*-factor × Sensitivity |
|---|---|---|---|
| SPR[5] | ~10 | 2600 | $2.6\times10^4$ |
| Localized SPR[6] | 136 | 1015 | $1.4\times10^5$ |
| Microring resonator[7] | $1.2\times10^4$ | 140 | $1.7\times10^6$ |
| Optical fiber sensor[8] | $5.2\times10^3$ | 172 | $8.9\times10^5$ |
| Photonic crystal[2] | 850 | 212 | $1.8\times10^5$ |
| Self-referencing ECL[3] | $2.8\times10^7$ | 212 | $5.9\times10^9$ |

Summary of the refractive index sensitivities and figure of merit (FOM) values of a variety of optical biosensor technologies. As a widely adopted metric for the intrinsic resolving power of optical biosensors, FOM incorporates the detection sensitivity *S* (nm· $RIU^{-1}$) and the resonant quality factor *Q* and is defined as FOM= $S\times Q$. The prism coupled SPR biosensor within the Biacore instrument has a FOM value of $2.6\times10^4$,[5] while an ECL laser has a value of $5.9\times10^9$,[3] indicating that the ECL biosensor has intrinsically better ability to resolve small changes in surface-adsorbed refractive index changes than SPR.

**Reference:**


(1) Wiechmann, S.; Müller, J. *Thin Solid Films* **2009**, *517*, 6847.

(2) Cunningham, B. T.; Qiu, J.; Li, P.; Lin, B. *Sens. Actuators. B Chem.* **2002**, *87*, 365.

(3) Ge, C.; Lu, M.; George, S.; Flood, T. A.; Wagner, C.; Zheng, J.; Pokhriyal, A.; Eden, J. G.; Hergenrother, P. J.; Cunningham, B. T. *Lab Chip* **2013**, *13*, 1247.

(4) Zhang, J.-H.; Chung, T. D. Y.; Oldenburg, K. R. *J. Biomol. Screen.* **1999**, *4*, 67.

(5) Homola, J. In *Optical Sensors*; Springer Berlin Heidelberg: 2004; Vol. 1, p 145.

(6) Shen, Y.; Zhou, J.; Liu, T.; Tao, Y.; Jiang, R.; Liu, M.; Xiao, G.; Zhu, J.; Zhou, Z.-K.; Wang, X.; Jin, C.; Wang, J. *Nat. Commun.* **2013**, *4*, 2381.

(7) Yalcin, A.; Popat, K. C.; Aldridge, J. C.; Desai, T. A.; Hryniewicz, J.; Chbouki, N.; Little, B. E.; King, O.; Van, V.; Sai, C.; Gill, D.; Anthes-Washburn, M.; Unlu, M. S.; Goldberg, B. B. *IEEE J. Sel. Top. Quant. Electron.* **2006**, *12*, 148.

(8) Chen, N.; Yun, B.; Cui, Y. *Appl. Phys. Lett.* **2006**, *88*, 133902.